Available online at www.sciencedirect.com
ScienceDirect
Journal of the European Ceramic Society 30 (2010) 971–979
www.elsevier.com/locate/jeurceramsoc

Compositional range and electrical properties of the morphotropic phase boundary in the $Na_{0.5}Bi_{0.5}TiO_3$–$K_{0.5}Bi_{0.5}TiO_3$ system

M. Otoničar*, S.D. Škapin, M. Spreitzer, D. Suvorov

Jožef Stefan Institute, Jamova 39, SI-1000 Ljubljana, Slovenia

Received 24 April 2009; received in revised form 18 September 2009; accepted 9 October 2009
Available online 13 November 2009

Abstract

We have investigated the $Na_{0.5}Bi_{0.5}TiO_3$–$K_{0.5}Bi_{0.5}TiO_3$ (NBT–KBT) system, with its complex perovskite structure, as a promising material for piezoelectric applications. The NBT–KBT samples were synthesized using a solid-state reaction method and characterized with XRD and SEM. Room-temperature XRD showed a gradual change in the crystal structure from tetragonal in the KBT to rhombohedral in the NBT, with the presence of an intermediate morphotropic region in the samples with a compositional fraction x between 0.17 and 0.25. The fitted perovskite lattice parameters confirmed an increase in the size of the crystal lattice from NBT towards KBT, which coincides with an increase in the ionic radii. Electrical measurements on the samples showed that the maximum values of the dielectric constant, the remanent polarization and the piezoelectric coefficient are reached at the morphotropic phase boundary (MPB) ($\varepsilon = 1140$ at 1 MHz; $P_r = 40\ \mu C/cm^2$; $d_{33} = 134$ pC/N).

Keywords: $Na_{0.5}Bi_{0.5}TiO_3$–$K_{0.5}Bi_{0.5}TiO_3$; Sintering; Microstructure; Morphotropic phase boundary (MPB); Electrical properties

1. Introduction

Piezoelectric materials are used in the electronics industry for various devices, such as sensors, actuators, transducers, etc. These devices exploit the piezoelectric properties, i.e., generating an electrical potential in response to a mechanical stress (direct effect), or inversely, they can generate a mechanical force in response to a voltage (inverse effect). Such materials are most often based on lead (e.g., $PbZr_xTi_{1-x}O_3$), which is a volatile transition-metal element, toxic to humans and the environment. Therefore, research on new piezomaterials is gradually turning to the development of lead-free piezoelectrics. An appropriate alternative to piezoelectric materials containing lead could be systems in the form of solid solutions with complex perovskite structures.[1,2]

Among the potential materials that could substitute for lead-based piezoelectric ceramics are $Na_{0.5}Bi_{0.5}TiO_3$- and $K_{0.5}Na_{0.5}NbO_3$-based perovskite materials.[3–7] The electrical properties of these two compounds can be modified by the formation of solid solutions with $K_{0.5}Bi_{0.5}TiO_3$,[8,9] $BaTiO_3$,[10,11] $SrTiO_3$,[12,13] $CaTiO_3$,[14] $NaTaO_3$,[15,16] $LiTaO_3$,[5,17] $LiNbO_3$,[18] $LiSbO_3$, etc.,[19] where the A- or B-site cations in the ABO_3 structure are substituted. Such substitutions result in lattice distortions due to the different sizes of the cations, which can cause a shift in the temperature-dependent polymorphic phase transitions, or can trigger the formation of a morphotropic phase boundary (MPB), where two different structures coexist. It is known from the literature that materials in the vicinity of polymorphic phase transitions, or in the MPB regions, exhibit enhanced electromechanical coupling properties.[1,2]

Many studies have been made on B-site cation-substituted perovskites, whereas A-site cation-substituted perovskites are relatively less investigated, but nevertheless important, since alkali cations contribute to the greater polarizability of the materials. $Na_{0.5}Bi_{0.5}TiO_3$ (NBT) is an A-site cation-substituted perovskite, which was first reported by Smolenskii and Agranovskaya in 1960.[20] It has complex perovskite structures with various crystallographic modifications and their associated phase-transition temperatures.[21] $K_{0.5}Bi_{0.5}TiO_3$ (KBT) ceramics, on the other hand, were only recently revealed to be potentially useful for selected applications. Therefore, many details about the crystal structure of KBT and its properties at various temperatures remain unresolved and are still the subject of investigations.

* Corresponding author. Tel.: +386 1 477 3991; fax: +386 1 477 3875.
E-mail address: mojca.otonicar@ijs.si (M. Otoničar).

0955-2219/$ – see front matter © 2009 Elsevier Ltd. All rights reserved.
doi:10.1016/j.jeurceramsoc.2009.10.006

NBT and KBT are relaxor ferroelectric materials that upon cooling undergo phase transitions to lower-ordered states.[21–27] Upon cooling, NBT transforms from a paraelectric cubic to a ferrielectric tetragonal structure over the temperature interval 540–500 °C, with an intermediate coexistence of the cubic and tetragonal structures. With further cooling the tetragonal structure changes to a ferroelectric rhombohedral structure over a wide temperature interval between 400 and 255 °C, where there is another region of coexistence of the tetragonal and rhombohedral structures.[21] The high-temperature tetragonal structure of NBT is in some articles reported to be antiferroelectric[6,12]; however, various measurements tend to contradict this statement, as a weak polarity was observed.[22,28] KBT, on the other hand, upon cooling undergoes a phase transformation from paraelectric cubic to a pseudocubic structure at approximately 410 °C, and subsequently to a ferroelectric tetragonal structure at approximately 270 °C.[25] The pseudocubic phase is believed to be a region of coexisting cubic and tetragonal structures, although some authors state that above 250 °C the structure already changes from tetragonal to cubic,[26] or that it changes to another intermediate tetragonal structure and then to a cubic one.[27] Permittivity measurements clearly demonstrated the relaxor properties in the high-temperature polymorphic regions of the described perovskites.

Some research was also performed on the $(1-x)Na_{0.5}Bi_{0.5}TiO_3 - xK_{0.5}Bi_{0.5}TiO_3$ (NBT–KBT) system; however, different groups used various synthesis procedures and therefore the determined structure and the resulting electrical properties are diverse. The NBT–KBT system is reported to form solid solutions with a morphotropic phase boundary (MPB) in a defined concentration range, showing improved electrical properties compared to NBT and KBT.[8,9,29–32] The structure of NBT–KBT was thoroughly examined using a Rietveld neutron powder profile analysis in the KBT concentration range (x) from 0 to 1 and in the temperature range from room temperature to 720 °C,[33] and with an X-ray absorption fine structure (XAFS) analysis.[34] The NBT–KBT solid solutions have a complex perovskite structure with the general formula $(A,A')_{0.5}A''_{0.5}BX_3$. The atoms are arranged so that A, A′ and A″ are occupied by Na^+, K^+ and Bi^{3+} as the A-site cations in the $A^{2+}B^{4+}O_3$ perovskite structure, whereas Ti^{4+} ions occupy the B-sites and are octahedrally coordinated with O^{2-} ions, which occupy the X-site in the structure. In the NBT–KBT system the atomic ratio between the Bi^{3+} and the (Na^+,K^+) atoms is always 1. The variable in the structure is, therefore, the ratio between the Na^+ and the K^+, where an important factor is their ability to substitute isovalently, so as to be efficiently distributed throughout the structure.

At room temperature, NBT crystallizes with a rhombohedral symmetry and the space group *R3c*, whereas KBT crystallizes with a tetragonal symmetry and the space group *P4mm* (from the ICSD database numbers 280983, SG No. 161, and 98057, SG No. 99, respectively).[21,33] In a certain concentration range of the NBT and KBT compounds there is a region where the tetragonal and rhombohedral structures coexist. For this reason the phase transitions in the NBT–KBT solid solutions are alkali-element-concentration and temperature dependent. However, the ratio between the NBT and the KBT in the samples at which the MPB region exists remains the main topic of discussion, since various authors reported different results.[8,9,23,27,31–33,35] Sasaki et al.[9] claimed that the MPB exists near the composition $x = 0.16$–0.20 in the $(Na_{1-x}K_x)_{0.5}Bi_{0.5}TiO_3$ system. Elkechai et al.[8] found a broader biphasic range, i.e., between $x = 0.08$ and 0.30, while Pronin et al.[27] determined a pseudocubic phase in the interval between $x = 0.18$ and 0.40. In the structural study of the NBT–KBT system performed by Jones et al.[33] no MPB was observed, only an intermediate rhombohedral structure with the space group *R3m* for $x = 0.50$ and 0.60. Previously, Kreisel et al.[35] determined an intermediate phase between $x = 0.50$ and 0.80 and no MPB region. In all the mentioned studies quite different reaction conditions were used, which could be the reason for the variation in the reports.

We focused our research on the two-component system $(Na_{1-x}K_x)_{0.5}Bi_{0.5}TiO_3$, which exhibits ferroelectric and piezoelectric properties over a broad concentration range around room temperature, and therefore seems to be an appropriate material for piezoelectric applications. The literature data are mostly contradictory in the concentration range of the existing morphotropic region, where the NBT–KBT solid solutions have the highest remanent polarization, and the highest piezo-response. The present investigation was, therefore, aimed to (i) develop optimal synthesis processes for making NBT–KBT ceramics, (ii) characterize the microstructure and the crystal structure of the samples across the whole concentration range at room temperature, and (iii) determine the dependence of the electrical properties on the structure. Thus, this investigation could serve as the basis for further research on the compositional modifications of NBT-based piezoelectrics.

2. Experimental

2.1. Sample preparation

Ceramic samples in the form of solid solutions with various fractions of NBT and KBT were prepared by a solid-state reaction method. The prepared samples with the general formula $(Na_{1-x}K_x)_{0.5}Bi_{0.5}TiO_3$ with different values of compositional fractions (x) are shown in Table 1.

As starting materials for preparing the ceramics reagent-grade powders (Alfa Aesar) of Na_2CO_3 (99.997%), K_2CO_3 (99.997%), Bi_2O_3 (99.975%) and TiO_2 (99.99%) were used in stoichiometric amounts. Both carbonates were previously dried at 200 °C for 2 h in order to remove any water content. The mixtures of powders were homogenized in a mortar with ethanol as a medium and then milled in a planetary ball mill at 200 rpm for 1 h using yttria-stabilized zirconia balls in ethanol. The milled powders were dried, uniaxially pressed into pellets at 100 MPa and then placed into a tube furnace, where they were calcined in air at 750 °C for 10 h. After the first calcination the pellets increased in volume by 12–16%. The pellets were then pulverized and X-ray powder diffraction (XRD) analyses were performed. The powder was then again pressed into pellets and calcined at 850 °C for 10 h to complete the reaction. The relatively low calcination temperatures are due to the low melting points of Na_2CO_3 (851 °C) and Bi_2O_3 (825 °C). After the second calcination the

Table 1
The compositional fractions of x in the $(Na_{1-x}K_x)_{0.5}Bi_{0.5}TiO_3$ solid-solution system, the associated sample label and the sintering temperatures of the samples.

Compositional fraction x in $(Na_{1-x}K_x)_{0.5}Bi_{0.5}TiO_3$	Sample label	Sintering temperature [°C]
0.00	NBT	1100
0.10	90NBT–10KBT	1100
0.15	85NBT–15KBT	1120
0.17	83NBT–17KBT	1120
0.20	80NBT–20KBT	1100
0.22	78NBT–22KBT	1100
0.25	75NBT–25KBT	1100
0.30	70NBT–30KBT	1090
0.50	50NBT–50KBT	1070
1.00	KBT	1030

pellets were observed to have shrunk by a few percent. The pellets were again pulverized and XRD analyses were made, while the remaining powder was milled in a planetary mill at 200 rpm for 1 h before further sintering.

The sintering curves for each of the samples were obtained using a heating microscope (EM 201, Hesse Instruments, Osterode, Germany) with a constant heating rate of 10 °C/min. From the sintering curves we determined the sintering temperatures (Table 1). The powders were then uniaxially pressed into pellets of various dimensions, for the purpose of different analyses, and cold isostatically pressed at 750 MPa. The pellets were placed into a tube furnace and sintered in air for 5 h at the sintering temperatures characteristic for each composition (1030–1120 °C). After sintering the pellets were cooled down together with the furnace. The measured shrinkage of the pellets was 16–19%. The density of the samples was measured in accordance with Archimedes' principle, using ethanol as the immersion fluid.

2.2. Characterization

The phase composition and the crystallinity of the samples were determined by XRD analyses after each heat treatment, using an X-ray powder diffractometer with Cu Kα radiation with an additional Johannson's monochromator in order to remove the Cu Kα$_2$ radiation. XRD patterns were recorded at room temperature in the 2θ range from 20° to 90° with a step size of 0.017° and a time of 4 s/step. The diffractograms were analyzed using EVA software (Bruker AXS) to define the phase composition. The structural analyses for determining the lattice parameters were made according to the whole-pattern decomposition method using TOPAS-R software (Bruker AXS).

Scanning electron microscopy (SEM; JXA 840A, JEOL, Tokyo) was used to determine the microstructural features of the samples, which were previously polished and coated with carbon. For the purpose of the grain-size determination the samples were thermally etched at 50 °C below the sintering temperature for 10 min and a field-emission-gun SEM (FE-SEM SUPRA 35VP, Carl Zeiss) was used to scan the surface. Next, Image Tool software was used to measure the mean diameter of the grains. The chemical composition of the phases was determined by energy-dispersive X-ray spectroscopy (EDS) and software (Series II X-ray microanalyzer, Tracor Northern, Middleton, WI), which gives a local elemental composition of the individual phases.

In order to measure the dielectric, ferroelectric and piezoelectric properties, different sizes of capacitors were made by applying silver electrodes on both sides of the pellets, drying, and then firing at 550 °C for 15 min.

The capacitance and dielectric losses of the samples were measured at frequencies of 1 kHz, 10 kHz, 100 kHz and 1 MHz in the temperature range from 0 to 600 °C using an LCR meter (Agilent 4284A; Agilent Technologies, Inc., Santa Clara, CA) and a chamber furnace. The dielectric constants were calculated from the measured values of the capacitance (C_p). For measuring the dependence of the polarization on the electric field a Radiant Technology test system (Precision LC 10V, Mineola, NY) and an amplifier (Trek, 10 kV) were used. The samples were exposed to an alternating voltage of up to ±4.5 kV in order to obtain hysteresis loops of the polarization versus the electric field at room temperature and at a frequency of 10 Hz. The value of the applied voltage depends on the thickness of the capacitors and corresponds to the applied electric field of 90 kV/cm. Prior to measuring the piezoelectricity of the samples they were poled in silicon oil in an electric field of 50 kV/cm at a temperature of 100 °C for 10 min. A piezometer (PiezoMeter System PM10, Take Control, Birmingham, UK) was then used to measure the d_{33} piezoelectric coefficient at room temperature and at a constant frequency of 100 Hz.

3. Results and discussion

The XRD analyses were made after each heat treatment in order to determine the phase composition and the crystal symmetry of the NBT–KBT samples. The XRD patterns of all the samples after the first calcination showed a single-phase composition, indicating that the reagents were already reacted to form the end compounds, releasing CO_2 from the carbonates. However, the structure was not perfectly ordered, as the peaks were wide and their intensities were low. During the second calcination the possible remaining reactants combined and the XRD patterns showed narrower and sharpener peaks with higher intensities. Fully dense samples were achieved by additional sintering of the pellets, which also resulted in single-phase compositions, according to the XRD patterns.

It is clear from the XRD patterns that the positions of the peaks change with the composition, gradually shifting towards lower angles with the addition of KBT to the NBT–KBT system. This indicates that the dimensions of the unit cells change, increasing from NBT towards KBT. As the theoretical coordination number of the A-site cations in the perovskite lattice is 12, the associated ionic radii are 1.39 Å for Na^+, 1.78 Å for K^+[36] and 1.34 Å for Bi^{3+}.[37] The difference in the sizes of the A-site cations of both the end-members, NBT and KBT, was calculated from the stated ionic radii and amounts to 0.195 Å. This difference in ionic radii is in accordance with the changes in the unit-cell dimensions of the NBT–KBT solid

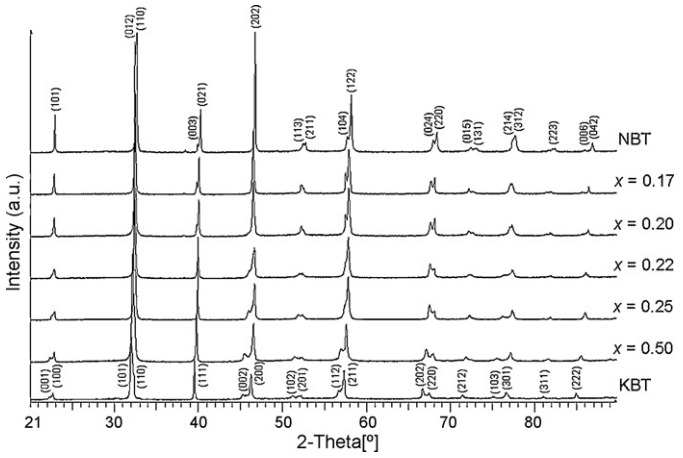

Fig. 1. XRD patterns of all the NBT–KBT samples, showing a change in the symmetry and the dimensions of the unit cells from tetragonal in KBT towards rhombohedral in NBT.

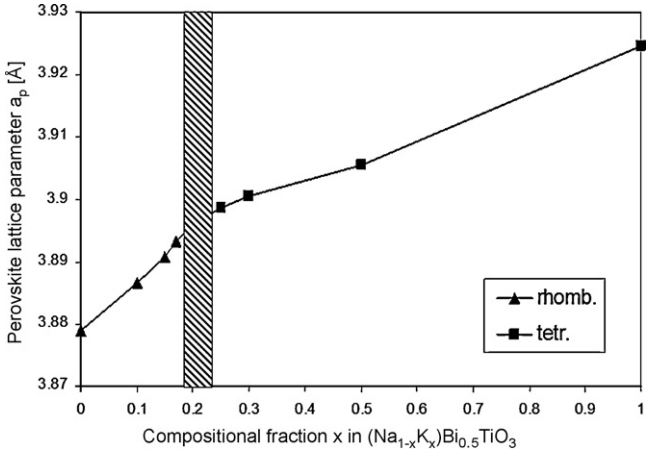

Fig. 3. The dependence of the perovskite unit-cell parameter a_P of the compositional fraction x in the $(Na_{1-x}K_x)_{0.5}Bi_{0.5}TiO_3$ solid-solution system 10 μm.

solutions, where the unit cell increases from NBT towards KBT.

The XRD patterns of the $(Na_{1-x}K_x)_{0.5}Bi_{0.5}TiO_3$ solid solutions imply that the samples with the compositions $x = 0$–0.17 show peaks characteristic for rhombohedral symmetry and the samples with the compositions $x = 0.25$–1 show peaks characteristic for tetragonal symmetry (Fig. 1). A detailed XRD scan revealed that at the compositions $x = 0.2$ and 0.22 the peaks of both tetragonal and rhombohedral symmetry are present in the XRD patterns, indicating that both structures coexist. The described phase transition with the intermediate MPB is represented in Fig. 2 by the peaks at 2θ angles around 40° and 46°.

The unit-cell parameters for each composition were determined by fitting the XRD patterns of the samples. The structures of both end-members, NBT and KBT, were taken as reference structures that become distorted upon the addition of K^+ or Na^+, respectively. Therefore, the rhombohedral *R3c* space group with hexagonal lattice parameters[21] was used for fitting the samples with the compositions $x = 0$–0.17, whereas the tetragonal *P4mm* space group[33] was used for fitting the samples with the compositions $x = 0.25$–1. The parameters of the reference structures taken from the ICSD card, however, do not fully coincide with the parameters of the synthesized NBT and KBT, which were therefore fitted. For the samples with the morphotropic phase at the compositions $x = 0.2$ and 0.22 the parameters of the *R3c* and *P4mm* structures were simultaneously used for the fitting, which resulted in the smallest error in the fitting of the lattice parameters compared to the other samples. The fitted dimensions of the unit cells and the corresponding perovskite lattice parameters (a_P) are given in Table 2. For the rhombohedral symmetry the perovskite unit-cell parameter a_{P_R} was calculated from equation $a_{P_R} = a_H/\sqrt{2}$, since the hexagonal unit-cell parameter a_H represents a face diagonal in the perovskite lattice.[38] The tetragonal unit-cell parameter a_T already represents the perovskite unit-cell parameter a_{P_T}, as the tetragonal lattice is elongated along the *c*-axis. Fig. 3 shows the graph of an increasing perovskite lattice

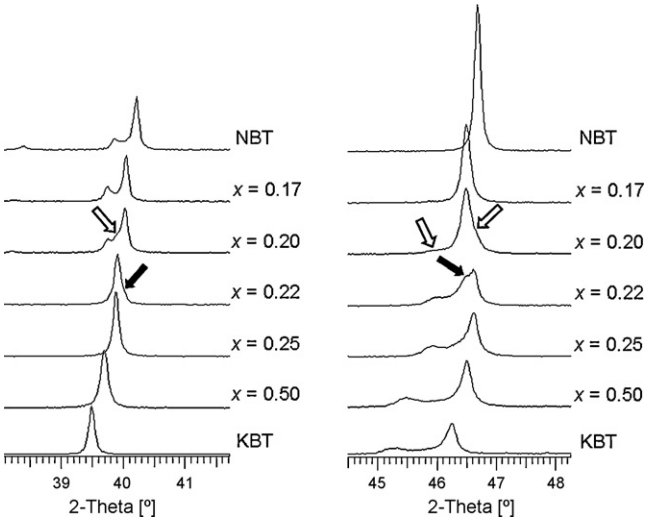

Fig. 2. XRD patterns of the samples across the MPB at 2θ angles around 40° and 46°. The arrows represent the peaks of the tetragonal (white) and rhombohedral (black) structures, indicating the morphotropic region.

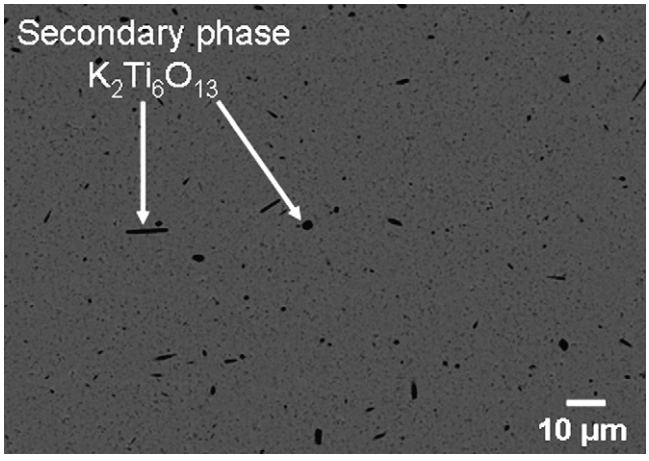

Fig. 4. Polished surface of the 80NBT–20KBT sample, showing a matrix phase with a small amount of a secondary phase $K_2Ti_6O_{13}$ in the form of elongated grains.

Table 2
The fitted hexagonal and tetragonal lattice parameters and the calculated perovskite lattice parameters of the rhombohedral and tetragonal solid solutions.

Compositional fraction x in $(Na_{1-x}K_x)_{0.5}Bi_{0.5}TiO_3$	a_H (Å)	c_H (Å)	V_H (Å^3)	a_{P_T} (Å)	c_T (Å)	V_T (Å^3)	a_{P_R} (Å)
0.00	5.4856(0)	13.5402(1)	352.86	–	–	–	3.8789
0.10	5.4963(9)	13.5718(3)	355.08	–	–	–	3.8865
0.15	5.5023(4)	13.5830(0)	356.09	–	–	–	3.8907
0.17	5.5059(7)	13.5878(7)	356.74	–	–	–	3.8933
0.20	5.5081(2)	13.6008(3)	357.36	3.8911(2)	3.9298(2)	59.50	3.8948
0.22	5.5189(1)	13.5557(0)	357.57	3.8897(4)	3.9425(9)	59.65	3.9025
0.25	–	–	–	3.8987(4)	3.9428(9)	59.93	–
0.30	–	–	–	3.9005(3)	3.9504(9)	60.10	–
0.50	–	–	–	3.9054(5)	3.9800(3)	60.71	–
1.00	–	–	–	3.9247(0)	3.9844(3)	61.37	–

parameter a_P from NBT towards KBT, which is in accordance with the average increase in the ionic radii.

SEM micrographs reveal that the samples consist of a predominant matrix phase and traces of a secondary phase (Fig. 4). It is clear from the images of the thermally etched samples that the grain size ranges from smaller to larger grains, with a random distribution within each sample (Fig. 5). Comparing the average grain size of all the samples it can be concluded that the grain size increases from 130 ± 70 nm in the KBT end-member towards 7.8 ± 3.2 μm in the NBT end-member. However, by decreasing the compositional fraction x the grain growth becomes more rapid and the grain size increases exponentially as the composition moves closer to that of NBT. The largest grains are observed in the NBT samples. Therefore, the smallest amount of KBT in the NBT–KBT solid solutions inhibits the grain growth.

The measured density of the solid-solution samples increased from 5.62 g/cm^3 for KBT towards 5.86 g/cm^3 for NBT. In comparison with the calculated theoretical values, where the density of KBT is 5.95 g/cm^3 and the density of NBT is 5.98 g/cm^3, the measured density of the samples ranged from 95 to 98% of the theoretical density. The pores were not connected to each other and were formed at the boundaries between the grain s, giving intergranular porosity.

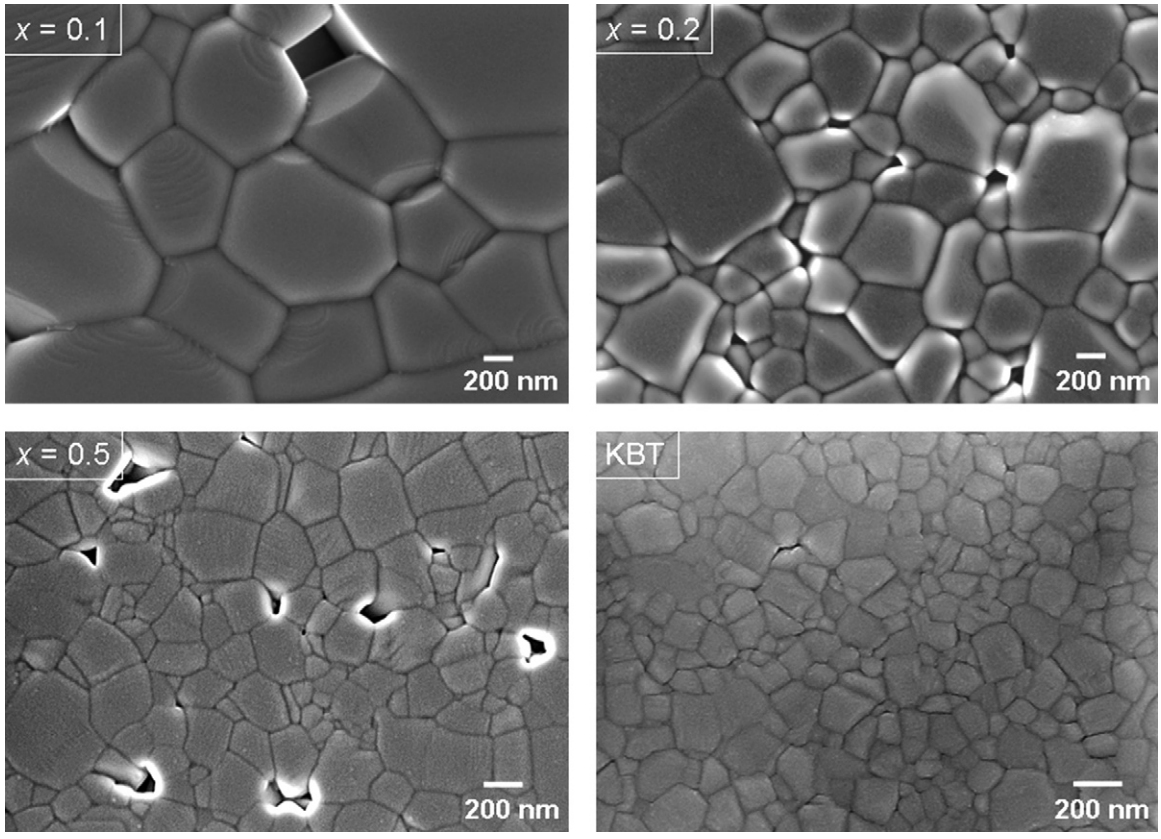

Fig. 5. Thermally etched surfaces of the $(Na_{1-x}K_x)_{0.5}Bi_{0.5}TiO_3$ samples with compositional fractions $x = 0.1$, 0.2, 0.5 and 1.0, showing an increasing grain size from KBT towards NBT.

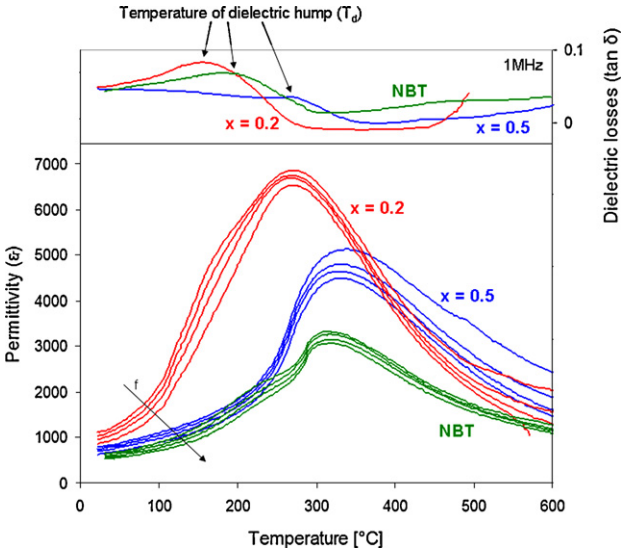

Fig. 6. Temperature dependence of permittivity and dielectric losses of the $(Na_{1-x}K_x)_{0.5}Bi_{0.5}TiO_3$ solid-solution samples with the compositional fractions $x = 0.0$, 0.2 and 0.5. The permittivity measurements were obtained at frequencies of 1 kHz, 10 kHz, 100 kHz and 1 MHz, whereas the dielectric losses are presented at 1 MHz. The values of permittivity decrease with increasing frequency for each sample analyzed.

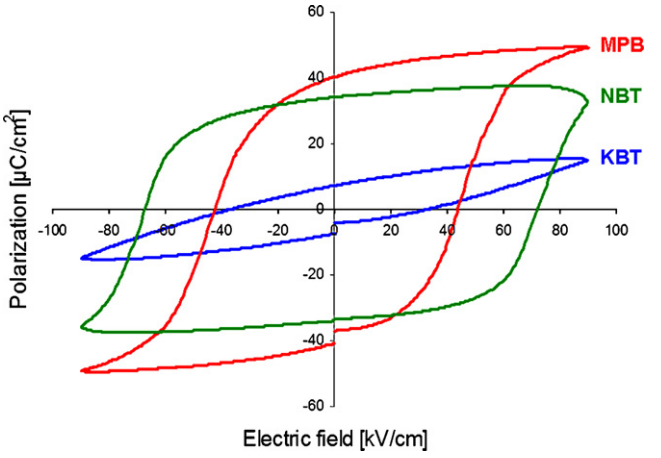

Fig. 7. Hysteresis loops of the $[(Na_{1-x}K_x)_{0.5}Bi_{0.5}TiO_3]$ solid-solution samples with the compositional fractions $x = 0.0$, 0.2 and 1.0. The NBT hysteresis is undersaturated.

EDS was used to determine the elemental compositions of the phases and to verify the stoichiometry of the solid solutions. The compositions of the matrix phases deviated slightly from the nominal starting compositions, most likely due to the formation of secondary phases and due to the evaporation of the bismuth and potassium components during the thermal treatment of the samples.[39,40] SEM micrographs show traces of a secondary phase in the form of elongated grains that are present in most of the samples, although the amount is most probably too small to be detected with the XRD analyses. EDS analyses confirmed the secondary phase to be potassium titanate ($K_2Ti_6O_{13}$), which matches the data reported on thermally treated KBT.[40,24]

The results of the dielectric properties confirmed the literature data on the characteristics of the NBT–KBT perovskite system.[41,42] The values of the relative dielectric permittivity and the dielectric losses at various frequencies for the samples with the compositional fractions $x = 0.0$, 0.2 and 0.5 are shown in Fig. 6. The measured values and the temperature of the permittivity maximum (ε_{max}, T_{max}), the dielectric losses ($\tan\delta$), and the temperature of the dielectric hump (T_d) change as the composition of the samples changes. By decreasing the compositional fraction x, the value of the permittivity maximum increases from KBT ($\varepsilon_{max} = 3820$ at 1 MHz) towards the samples with the MPB, reaching the highest value at $x = 0.2$ ($\varepsilon_{max} = 6540$ at 1 MHz). With a further decrease of x towards NBT, the value of the permittivity maximum decreases down to $\varepsilon_{max} = 3070$ (at 1 MHz). The opposite trend is noticed for the lowest values of the dielectric losses ($\tan\delta$), which coincide with the maximum permittivity. Furthermore, the maximum temperature decreases from 380 °C for KBT to 270 °C for the sample with the MPB at $x = 0.2$, and increases again to 320 °C for NBT. The temperature of the frequency-dispersive dielectric hump is clearly demonstrated by the local maximum in the dielectric losses, which in the case of NBT indicates the temperature of the ferroelectric decay, when a domain-structured ferroelectric transforms to a polymorphic state. The dielectric hump temperature in all the samples is relatively high, making the investigated system appropriate for many applications. The temperature of the dielectric hump decreases with the decreasing compositional fraction x from KBT ($T_d \approx 280$ °C) towards the sample with the MPB at $x = 0.2$ ($T_d \approx 155$ °C), and increases with the further decrease of x to the NBT end-member ($T_d \approx 185$ °C). However, the opposite is true for the value of the dielectric-loss maximum, which increases from KBT to the MPB at $x = 0.2$ and decreases towards NBT. The samples at the MPB therefore exhibit the highest permittivity-maximum values, the lowest values of the dielectric-loss minimum at T_m, the lowest temperatures of the dielectric anomalies (T_m and T_d) and the highest values of the dielectric-loss maximum at T_d. The same trend as for permittivity versus temperature is also seen at room temperature, where the highest values of the permittivity are reached for the samples with the MPB ($\varepsilon = 1140$ at 1 MHz) (Table 3).

Room-temperature measurements of the polarization versus electric field were performed on the samples in order to determine the value of the coercive electric field (E_c) and the remanent polarization (P_r), characteristic for ferroelectric materials (Fig. 7). The samples were exposed to a frequency of 10 Hz and to an external electric field of up to 90 kV/cm. Higher values of applied voltage caused the samples to undergo a dielectric breakdown due to the brittle nature of the materials, which could be attributed to defects in the crystal structure. For comparison reasons, the hysteresis of the NBT sample was measured in the same range of electric field (±90 kV/cm), although the material had not yet reached its saturation polarization. By comparing the hysteresis loops of all the samples we can see that a decrease in the compositional fraction x in the materials causes an increase in the remanent polarization from 7 μC/cm² for KBT to 40 μC/cm² for the MPB sample at $x = 0.2$. A further decrease of P_r can be observed for a compositional change from the MPB towards NBT, where the remanent polarization reaches 34 μC/cm². The values of the coercive electric field, on the other hand, increase

Table 3
The values of the relative dielectric constant, dielectric loss, remanent polarization, coercive field and piezoelectric constant for the samples with different compositional fractions x in the $(Na_{1-x}K_x)_{0.5}Bi_{0.5}TiO_3$ ceramics at room temperature.

Compositional fraction x in $(Na_{1-x}K_x)_{0.5}Bi_{0.5}TiO_3$	ε_r	$\tan\delta$	P_r [μC/cm^2]	E_c [kV/cm]	d_{33} [pC/N]
0.00	536	0.0490	34	72	68
0.10	555	0.0504	40	56	102
0.15	695	0.0537	40	48	108
0.17	725	0.0554	40	46	112
0.20	1140	0.0765	40	44	134
0.22	1015	0.0757	35	35	126
0.25	965	0.0755	28	36	107
0.30	805	0.0727	24	37	100
0.50	640	0.0541	20	44	90
1.00	530	0.0720	7	33	24

from KBT (E_c = 33 kV/cm) towards the sample with the MPB (E_c = 44 kV/cm) and further on towards NBT (E_c = 72 kV/cm) (Table 3).

The highest values of remanent polarization for the MPB samples can be attributed to the increased number of possible directions of polarization because of the coexistence of more than one anisotropic crystal structure (6 for tetragonal ⟨1 0 0⟩ and 8 for rhombohedral ⟨1 1 1⟩). Thus, the MPB composition enables the dipole moments to align efficiently with the field, resulting in a higher polarizability of the material.[43]

The piezoelectric measurements were performed on the previously poled samples, where the domains were switched so that the polarization has the same direction as the applied electric field. In the case of the NBT–KBT samples the piezoelectric constant d_{33} increases from KBT (d_{33} = 24 pC/N at 100 Hz) to the MPB sample at x = 0.2 (d_{33} = 134 pC/N at 100 Hz) and decreases again from the MPB sample towards NBT (d_{33} = 68 pC/N at 100 Hz) (Fig. 8, Table 3). The trend of an increasing piezoelectric constant towards the MPB was already demonstrated for other solid-solution systems, especially in the case of PZT.[1,2] The reason for the enhanced piezoelectric response at the MPB is in the easier dipole alignment due to the large number of possible directions of polarization, and this is the same for the highest remanent polarization of the material.

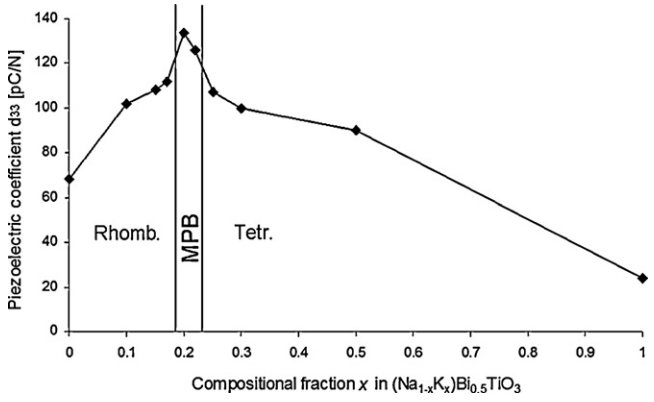

Fig. 8. Piezoelectric constant d_{33} of the $[(Na_{1-x}K_x)_{0.5}Bi_{0.5}TiO_3]$ samples, measured at 100 kHz at room temperature.

According to our experiences with the synthesis of NBT-based[16,44] and KBT[40] ceramics, the preparation conditions are very important because of the presence of highly volatile and hygroscopic elements. In the study of Elkechai et al.[8] the initial firing temperature, which was between 880 and 950 °C, was set above the melting temperature of some reagents, i.e., Bi_2O_3, Na_2CO_3 and K_2CO_3, which melt at 825, 851 and 891 °C, respectively. Moreover, for the preparation of single crystals by Jones et al.,[33] who found no MPB region, stoichiometric mixtures of reagents were directly exposed to temperatures as high as 1300 °C. In such conditions considerable weight losses might occur, which would result in stoichiometry and MPB-range variations. In contrast, Sasaki et al.,[9] who used similar reaction conditions to those in our study, also arrived at similar results related to the MPB range (x = 0.16–0.20). Thus, it appears that the structural characteristics of the samples from the investigated system strongly depend on their preparation conditions. Since the electrical properties, especially the piezoelectricity, are most pronounced for samples within the MPB range, this finding is also of practical importance.

4. Conclusions

In the present study, we analyzed the structural and electrical characteristics of the NBT–KBT system because of its potential as an alternative to piezoelectric materials that contain lead. Using XRD analyses we determined that the NBT–KBT perovskite system crystallizes in the form of solid solutions across a wide concentration range, with a narrow intermediate morphotropic region. The MPB region with its coexisting rhombohedral and tetragonal structures extends between the compositions x = 0.17 and 0.25 in the $(Na_{1-x}K_x)_{0.5}Bi_{0.5}TiO_3$ samples. The perovskite lattice parameters a_P of the NBT–KBT ceramics were calculated from the reference samples' lattice parameters and were shown to increase with the increasing compositional fraction x, which is consistent with the increase in the size of the ionic radii. The average grain size, on the other hand, decreases exponentially from the NBT (7.8 ± 3.2 μm) towards the KBT (130 ± 70 nm) component. The relative density of the samples also decreases from the NBT (98%) towards the KBT (95%) component. A high relative density indicates an effective sintering process for the ceramic samples,

and therefore credible results from the electrical measurements.

The samples with the MPB show improved ferroelectric and piezoelectric properties ($P_r = 40\,\mu C/cm^2$; $E_c = 44\,kV/cm$; $d_{33} = 134\,pC/N$) compared to the end-members, which can be attributed to the coexistence of various polarization axes because of the diverse distortions of the rhombohedral and tetragonal perovskite crystals. The dipole alignment with the electric field is, as a result, more efficient for the samples with the MPB and therefore contributes to larger values of polarization and electromechanical coupling.

Acknowledgement

The research was financially supported by the Ministry of Higher Education, Science and Technology of the Republic of Slovenia (Grant No. 1000-07-310059).

References

1. Jaffe, B., Cook Jr., W. R. and Jaffe, H., *Piezoelectric Ceramics*. Academic Press, London, 1971.
2. Cohen, R. E., Theory of ferroelectrics: a vision for the next decade and beyond. *J. Phys. Chem. Solid*, 2000, **61**, 139–146.
3. Shrout, T. R. and Zhang, S. J., Lead-free piezoelectric ceramics: alternatives for PZT? *J. Electroceram.*, 2007, **19**, 111–124.
4. Takenaka, T., Nagata, H. and Hiruma, Y., Current developments and prospective of lead-free piezoelectric ceramics. *Jpn. J. Appl. Phys.*, 2008, **47**, 3787–3801.
5. Saito, Y., Takao, H., Tani, T., Nonoyama, T., Takatori, K., Homma, T. *et al.*, Lead-free piezoceramics. *Nature*, 2004, **432**, 84–87.
6. Isupov, V. A., Ferroelectric $Na_{0.5}Bi_{0.5}TiO_3$ and $K_{0.5}Bi_{0.5}TiO_3$—perovskites and their solid solutions. *Ferroelectrics*, 2005, **315**, 123–147.
7. Gomah-Pettry, J. R., Saïd, S., Marchet, P. and Mercurio, J. P., Sodium–bismuth titanate based lead-free ferroelectric materials. *J. Eur. Ceram. Soc.*, 2004, **24**, 1165–1169.
8. Elkechai, O., Manier, M. and Mercurio, J. P., $Na_{0.5}Bi_{0.5}TiO_3$–$K_{0.5}Bi_{0.5}TiO_3$ (NBT–KBT) system: a structural and electrical study. *Phys. Status Solidi (A)*, 1996, **157**, 499–506.
9. Sasaki, A., Chiba, T., Mamya, Y. and Otsuki, E., Dielectric and piezoelectric properties of $(Bi_{0.5}Na_{0.5})TiO_3$–$(Bi_{0.5}K_{0.5})TiO_3$ systems. *Jpn. J. Appl. Phys.*, 1999, **38**, 5564–5567.
10. Takenaka, T., Maruyama, K. and Sakata, K., $(Bi_{1/2}Na_{1/2})TiO_3$–$BaTiO_3$ system for lead-free piezoelectric ceramics. *Jpn. J. Appl. Phys.*, 1991, **30**, 2236–2239.
11. Xu, Q., Chen, X., Chen, W., Chen, S., Kim, B. and Lee, J., Synthesis, ferroelectric and piezoelectric properties of some $(Na_{0.5}Bi_{0.5})TiO_3$ system compositions. *Mater. Lett.*, 2005, **59**, 2437–2441.
12. Sakata, K. and Masuda, Y., Ferroelectric and antiferroelectric properties of $(Na_{0.5}Bi_{0.5})TiO_3$–$SrTiO_3$ solid solution ceramics. *Ferroelectrics*, 1974, **7**, 347–349.
13. Wang, R., Xie, R. J., Hanada, K., Matsusaki, K., Bando, H. and Itoh, M., Phase diagram and enhanced piezoelectricity in the strontium titanate doped potassium–sodium niobate solid solution. *Phys. Status Solidi (A)*, 2005, **202**, R57–R59.
14. Bahuguna Saradhi, B. V., Srinivas, K. and Bhimasankaram, T., Electrical properties of $(Na_{1/2}Bi_{1/2})_{1-x}Ca_xTiO_3$ ceramics. *Int. J. Mod. Phys. B*, 2002, **16**, 4175–4187.
15. Iwasaki, H. and Ikeda, T., Studies on the system $Na(Nb_{1-x}Ta_x)O_3$. *J. Phys. Soc. Jpn.*, 1963, **18**, 157–163.
16. König, J., Jančar, B. and Suvorov, D., New $Na_{0.5}Bi_{0.5}TiO_3$–$NaTaO_3$-based perovskite ceramics. *J. Am. Ceram. Soc.*, 2007, **90**, 3621–3627.
17. Guo, Y., Kakimoto, K. and Ohsato, H., $(Na_{0.5}K_{0.5})NbO_3$–$LiTaO_3$ lead-free piezoelectric ceramics. *Mater. Lett.*, 2005, **59**, 241–244.
18. Guo, Y., Kakimoto, K. and Ohsato, H., Phase transitional behavior and piezoelectric properties of $(Na_{0.5}K_{0.5})NbO_3$–$LiNbO_3$ ceramics. *Appl. Phys. Lett.*, 2004, **85**, 4121–4123.
19. Zhang, S., Xia, R. and Shrout, T. R., Lead-free piezoelectric ceramics vs. PZT? *J. Electroceram.*, 2007, **19**, 251–257.
20. Smolenskii, G. A. and Agranovskaya, A. I., Dielectric polarization of a number of complex compounds. *Sov. Phys. Solid State*, 1960, **1**, 1429–1437.
21. Jones, G. O. and Thomas, P. A., Investigation of the structure and phase transitions in the novel A-site substituted distorted perovskite compound $Na_{0.5}Bi_{0.5}TiO_3$. *Acta Crystallogr.*, 2002, **B58**, 168–178.
22. Jones, G. O. and Thomas, P. A., The tetragonal phase of $Na_{0.5}Bi_{0.5}TiO_3$—a new variant of the perovskite structure. *Acta Crystallogr.*, 2000, **B56**, 426–430.
23. Jones, G. O., Kreisel, J., Jennings, V., Geday, M. A., Thomas, P. A. and Glazer, A. M., Investigation of a peculiar relaxor ferroelectric: $Na_{0.5}Bi_{0.5}TiO_3$. *Ferroelectrics*, 2002, **270**, 191–196.
24. Hiruma, Y., Aoyagi, R., Nagata, H. and Takenaka, T., Ferroelectric and piezoelectric properties of $(Bi_{1/2}K_{1/2})TiO_3$ ceramics. *Jpn. J. Appl. Phys.*, 2005, **44**, 5040–5044.
25. Ivanova, V. V., Kapyshev, A. G., Venevtsev, Y. N. and Zhdanov, G. S., X-ray determination of the symmetry of elementary cells of the ferroelectric materials $(K_{0.5}Bi_{0.5})TiO_3$ and $(Na_{0.5}Bi_{0.5})TiO_3$ and of high-temperature phase transitions in $(K_{0.5}Bi_{0.5})TiO_3$. *Izv. Akad. Nauk SSSR*, 1962, **26**, 354–356.
26. Li, Z. F., Wang, C. L., Zhong, W. L., Li, J. C. and Zhao, M. L., Dielectric relaxor properties of $K_{0.5}Bi_{0.5}TiO_3$ ferroelectrics prepared by sol–gel method. *J. Appl. Phys.*, 2003, **94**, 2548–2552.
27. Pronin, I. P., Parfenova, N. N., Zaitseva, N. V., Isupov, V. A. and Smolenskii, G. A., Phase transitions in solid solutions of sodium–bismuth and potassium–bismuth titanates. *Sov. Phys. Solid State*, 1982, **24**, 1060–1062.
28. Roleder, K., Franke, I., Glazer, A. M., Thomas, P. A., Miga, S. and Suchanicz, J., The piezoelectric effect in $Na_{0.5}Bi_{0.5}TiO_3$ ceramics. *J. Phys.: Condens. Matter*, 2002, **14**, 5399–5406.
29. Zhao, S., Li, G., Ding, A., Wang, T. and Yin, Q., Ferroelectric and piezoelectric properties of $(Na, K)_{0.5}Bi_{0.5}TiO_3$ lead free ceramics. *J. Phys. D: Appl. Phys.*, 2006, **39**, 2277–2281.
30. Yoshii, K., Hiruma, Y., Nagata, H. and Takenaka, T., Electrical properties and depolarization temperature of $(Bi_{1/2}Na_{1/2})TiO_3$–$(Bi_{1/2}K_{1/2})TiO_3$ lead-free piezoelectric ceramics. *Jpn. J. Appl. Phys.*, 2006, **45**, 4493–4496.
31. Baek, J., Kim, J. H., Khim, Z. G., Ahn, C. W., Kim, I. W. and Kim, H. W., Investigation of lead-free piezoceramics $Bi_{0.5}(Na_{1-x}K_x)_{0.5}TiO_3$ with scanning probe microscope. *J. Phys.: Confer. Ser.*, 2007, **61**, 545–549.
32. Zhang, Y. R., Li, J. F. and Zhang, B. P., Enhancing electrical properties in NBT–KBT lead-free piezoelectric ceramics by optimizing sintering temperature. *J. Am. Ceram. Soc.*, 2008, **91**, 2716–2719.
33. Jones, G. O., Kreisel, J. and Thomas, P. A., A structural study of the $(Na_{1-x}K_x)_{0.5}Bi_{0.5}TiO_3$ perovskite series as a function of substitution (x) and temperature. *Powder Diffr.*, 2002, **17**, 301–319.
34. Shuvaeva, V. A., Zekria, D., Glazer, A. M., Jiang, Q., Weber, S. M., Bhattacharya, P. *et al.*, Local structure of the lead-free relaxor ferroelectric $(K_xNa_{1-x})_{0.5}Bi_{0.5}TiO_3$. *Phys. Rev. B*, 2005, **71**, 174114.
35. Kreisel, J., Glazer, A. M., Jones, G., Thomas, P. A., Abello, L. and Lucazeau, G., An X-ray diffraction and Raman spectroscopy investigation of A-site substituted perovskite compounds: the $(Na_{1-x}K_x)_{0.5}Bi_{0.5}TiO_3$ ($0 \le x \le 1$) solid solution. *J. Phys.: Condens. Matter*, 2000, **12**, 3267–3280.
36. Shannon, R. D., Revised effective ionic radii and studies of interatomic distances in halides and chalcogenides. *Acta Crystallogr.*, 1976, **A32**, 751–767.
37. Eitel, R. E., Randall, C. A., Shrout, T. R., Rehrig, P. W., Hanckenberger, W. and Park, S. E., New high temperature morphotropic phase boundary piezoelectrics based on $Bi(Me)O_3$–$PbTiO_3$ ceramics. *Jpn. J. Appl. Phys.*, 2001, **40**, 5999–6002.
38. Mitchell, R. H., *Perovskites: Modern and Ancient*. Almaz Press, Ontario, 2002.
39. Zhao, S., Zhang, L., Li, G., Wang, T. and Ding, A., Dielectric properties of $Na_{0.25}K_{0.25}Bi_{0.5}TiO_3$ lead-free ceramics. *Phys. Status Solidi (A)*, 2005, **202**, R22–R24.

40. König, J., Spreitzer, M., Jančar, B., Suvorov, D., Samardžija, Z. and Popovič, A., The thermal decomposition of $K_{0.5}Bi_{0.5}TiO_3$ ceramics. *J. Eur. Ceram. Soc.*, 2008.
41. Saïd, S. and Mercurio, J. P., Relaxor behaviour of low lead and lead free ferroelectric ceramics of the $Na_{0.5}Bi_{0.5}TiO_3$–$PbTiO_3$ and $Na_{0.5}Bi_{0.5}TiO_3$–$K_{0.5}Bi_{0.5}TiO_3$ systems. *J. Eur. Ceram. Soc.*, 2001, **21**, 1333–1336.
42. Li, Y., Chena, W., Zhoua, J., Xua, Q., Suna, H. and Liao, M., Dielectric and ferroelectric properties of lead-free $Na_{0.5}Bi_{0.5}TiO_3$–$K_{0.5}Bi_{0.5}TiO_3$ ferroelectric ceramics. *Ceram. Int.*, 2005, **31**, 139–142.
43. Bhattacharya, K. and Ravichandran, G., Ferroelectric perovskites for electromechanical actuation. *Acta Mater.*, 2003, **51**, 5941–5960.
44. Spreitzer, M., Valant, M. and Suvorov, D., Sodium deficiency in $Na_{0.5}Bi_{0.5}TiO_3$. *J. Mater. Chem.*, 2007, **17**, 185–192.